



Understanding the effect of Pd size on formic acid dehydrogenation via size-controlled Pd/C catalysts prepared by NaBH₄ treatment

Yongwoo Kim, Do Heui Kim*

School of Chemical and Biological Engineering, Institute of Chemical Processes, Seoul National University, 1 Gwanak-ro, Gwanak-gu, Seoul, 08826, Republic of Korea



ARTICLE INFO

Keywords:
Formic acid dehydrogenation
Palladium
Size effect
Activation energy
Hydrogen production

ABSTRACT

Herein, we investigated the effect of Pd size on a formic acid dehydrogenation (FAD) reaction. A series of size-controlled Pd/C catalysts was simply prepared by a treatment using sodium borohydride (NaBH₄), which provides *in-situ* hydrogen in the aqueous phase. Pd particles in the catalyst were gradually aggregated as the number of NaBH₄ treatments increased, resulting in the synthesis of the size-controlled Pd/C catalysts with the Pd size from 2.5 nm to 4.8 nm. The catalytic activities of the size-controlled Pd/C catalysts continuously declined with increasing the Pd size, which was attributed to the decrease in the number of active sites of the catalyst. However, the decreasing trend of turnover frequency (TOF(h⁻¹)) values with the Pd size at low temperature demonstrated that the intrinsic activity of the small Pd is higher than that of the large Pd. More importantly, such decreasing trends of TOF values as a function of the Pd size gradually disappeared when raising the reaction temperature. It implies that there is a thermodynamic effect of the Pd size on the FAD reaction, which was evidenced by a continuous increase in the activation energy from 44.9 kJ/mol to 63.9 kJ/mol with the Pd size. We proposed that the H₂ desorption step is the rate-determining step for FAD reaction. Such proposal can explain the size-dependent catalytic activity and the increase in the activation energy of FAD with the Pd size enlargement, as the temperature programmed hydrogen decomposition (TPHD) analysis demonstrated that the large Pd particle requires a high temperature/energy to desorb hydrogen from Pd. Consequently, it is concluded that the size-dependent catalytic activity of FAD is attributed not only to the number of active sites but also to the thermodynamic factor relating to the rate-determining step.

1. Introduction

Formic acid (HCOOH) has attracted worldwide attention as a promising liquid hydrogen carrier due to its high hydrogen density (4.4 wt. %), non-toxicity, stability and sustainability. Typically, formic acid decomposes through a dehydrogenation reaction to generate hydrogen (H₂) and carbon dioxide (CO₂), which is HCOOH → H₂ + CO₂. On the other hand, a dehydration reaction of formic acid uncommonly occurs to produce water (H₂O) and carbon monoxide (CO), which is HCOOH → H₂O + CO. Since a fuel cell, one of the feasible systems to utilize formic acid as a hydrogen storage media, has poisoning issues of Pt-electrode arising from CO, a catalyst for formic acid dehydrogenation (FAD) should have high enough selectivity toward H₂ and CO₂, by restraining the dehydration reaction [1–3]. However, it seems relatively difficult to absolutely suppress the formation of CO under a gas phase reaction over various catalysts including Pd/C [4–7], whereas even a monometallic Pd/C catalyst had almost 100% H₂ selectivity for the aqueous phase reaction, at a temperature above 50 °C [8–10]. Thus,

from the perspective of the practical application, the aqueous phase reaction would be preferred due to the utility of liquid material, and its high selectivity toward H₂ and CO₂.

Several noble metals (e.g. Pd, Au and Ru) were suggested as active phases for the FAD reaction [7,10–14]. Since Pd is the most widely used metal for the aqueous reaction among them [15,16], numerous attempts have been made to improve the catalytic performance of Pd-based catalysts by modifying the physicochemical properties of the catalyst [17]. One is to synthesize a bimetallic or trimetallic Pd-based alloy prepared with Au, Ag, Ni or Co [18–27]. Another is to select diverse kinds of supports such as carbon, ceria, resin, metal-organic-framework, and zeolite, or to functionalize supports such as amine-functionalized silica, TiO₂-doped carbon, and MnO_x-doped amine-functionalized silica [9,10,28–36]. However, irrespective of the various methods used to enhance the catalytic activity, a size of Pd was generally designated as one of the most critical factors determining the performance of the catalyst [9,10,22,24,25,28–30,34,37]. Thus, several studies recently endeavored to examine the concrete effect of the Pd

* Corresponding author.

E-mail address: dohkim@snu.ac.kr (D.H. Kim).

size on the FAD reaction, but there are some unresolved issues [38–40]. For example, Yamashita et al. concluded that the active site of Pd is terrace site, while Lu et al. reported that all surface site is the active site, by adopting a cubooctahedron model [38,39]. Not only disagreement about the active site, but also their explanations were only focused on the reactions at near room temperature. Such approach obstructed the thermodynamic understanding of Pd size effect. In addition, Lu et al. and Cai et al. calculated TOF (h^{-1} , surface) values based on total surface Pd sites, and correlated the TOF (h^{-1} , surface) values with the Pd size [39,40]. Lu et al. observed the decreasing trend of the TOF (h^{-1} , surface) values as a function of the Pd size [39]. However, they considered that those values were relatively independent of the Pd size, because other TOF values calculated on the basis of terrace sites or edge and corner sites decreased far more steeply with the Pd size than the TOF (h^{-1} , surface) values [39]. On the other hand, Cai et al. also observed the decreasing trend of the TOF (h^{-1} , surface) values with the Pd size, and explained it by either CO poisoning effect or d-band shift effect, but evidence seemed insufficient [40]. Thus, the further and concrete explanations were required, including understanding the thermodynamic effect of the Pd size. This led us to investigate the Pd size effect on the FAD reaction at different temperatures. To this end, we adopted a new and facile preparation method to control the size of Pd without using any organic surfactant.

2. Experimental

2.1. Preparation of catalysts

2.1.1. Materials

Palladium(II) chloride ($\text{Pd}(\text{Cl})_2$), sodium carbonate (Na_2CO_3), sodium borohydride (NaBH_4), and formic acid (HCOOH , > 96%) were purchased from Sigma-Aldrich. Carbon support (Vulcan XC72) was obtained from Cabot Co., while sodium chloride (NaCl) was acquired from Samchun Pure Chemical Co. (Korea). All chemicals were used without any further purification. The Milli-Q water was obtained by distillation and deionization to maintain its resistivity at $18.2 \text{ M}\Omega \text{ cm}$. Sodium tetrachloropalladate (Na_2PdCl_4) solution was prepared by dissolving 1:2 M ratios of PdCl_2 and NaCl in Milli-Q water. The equipment for the synthesis, such as glassware and magnetic bar, was ultra-sonically cleaned with Milli-Q water, and then dried at 100°C in an oven.

2.1.2. Size-controlled Pd/C

Controlling the Pd size of Pd/C catalysts was carried out via step-wise preparations; synthesis of Pd/C and enlargement of the Pd size. The catalyst with the smallest Pd size was synthesized by applying a deposition-precipitation method. The carbon support (0.3 g) was well-dispersed in 40 mL of 4 mM Na_2CO_3 solution while stirring for 1 h. The concentration of Na_2CO_3 (4 mM) was determined to maximize the catalytic activity of synthesized Pd/C catalyst (Figure S1). Then, 4 mL of as-prepared Na_2PdCl_4 solution (0.05 M) was added into Na_2CO_3 solution for Pd^{2+} ion to be precipitated under vigorous stirring. After the precipitation of Pd^{2+} ion and the deposition of precipitate on the carbon support for 1 h, 25 mL of NaBH_4 solution (molar amount of 20 times Pd metal) was introduced dropwise into the previous solution to reduce Pd^{2+} to Pd metal. The suspension was stirred for an additional 1 h, and then filtered with 4 L of Milli-Q water to fully eliminate residual ions. Finally, the catalyst was used after drying under ambient atmosphere at 100°C for 16 h. The drying condition was strictly controlled, since the drying condition was the highest temperature where the catalyst was exposed during the synthetic process.

In order to enlarge the particle size of Pd, a new preparation method was proposed by adopting NaBH_4 as hydrogen (H_2) source, which can sinter Pd particles in aqueous solution. First, 0.5 g of Pd/C catalyst with the smallest Pd size was well-dispersed in 150 mL of Milli-Q water, and stirred vigorously at 60°C for 1 h. Then, 30 mL of NaBH_4 solution (molar amount of 20 times Pd metal) was added dropwise. After

additional stirring for 2 h, the suspension was filtered with 4 L of Milli-Q water for the complete elimination of the residual elements, such as sodium and boron. The catalyst was also dehydrated under ambient atmosphere at 100°C for 16 h. It was observed that only the number of NaBH_4 treatments could change the Pd size, while the concentration of NaBH_4 solution, reaction time and reaction temperature hardly influenced the Pd size (Figure S2). Therefore, the catalysts were treated with NaBH_4 several times to synthesize the various size-controlled Pd/C catalysts. The catalysts were designated as Pd/C-xT, where x is the number of NaBH_4 treatments.

2.2. Characterization

The content of Pd in the catalysts was determined by inductively coupled plasma atomic emission spectroscopy (ICP-AES). The catalysts were pretreated in aqua regia, which is a 3:1 volumetric mixture of HCl and HNO_3 at 95°C for 4 h, to completely dissolve Pd. The solution was filtered by a syringe filter, diluted in the detectable range, and then analyzed. The nitrogen adsorption-desorption isotherms were performed by using BELSORP-mini II at the temperature of -196°C (liquid N_2). All samples were pretreated at 120°C for 4 h while maintaining a vacuum condition to remove moisture and impurities. Then, the specific surface area was calculated by applying the Brunauer-Emmett-Teller (BET) method. The crystalline phase and the relative crystallite size of the catalysts were analyzed by X-ray diffraction (XRD) patterns, which were taken with the powder X-ray diffractometer (Smartlab, Rigaku) operated at a current of 30 mA and a voltage of 40 kV. The samples were finely ground before analysis, and measured in the scan range from 10 to 90° . The scan speed and scanning step size were $1.0^\circ/\text{min}$ and 0.2° , respectively, to record XRD patterns with high resolution. The images of morphologies and particles of the size-controlled Pd/C catalysts were collected by transmission electron microscope (Cs-TEM) equipped with cold field emission gun and spherical aberration corrector (JEM-ARM200 F) at the accelerating voltage of 200 kV. The particle size distributions and the average particle sizes of Pd were calculated by counting more than 200 particles in the 800k magnified TEM images. The metal dispersions of the size-controlled Pd/C catalysts were measured by pulsed CO chemisorption performed on BEL-CAT-II (BEL Japan Inc.). About 0.03 g of sample was pretreated under 5 vol.% H_2/Ar gas condition at 100°C for 0.5 h with a ramping rate of $10^\circ\text{C}/\text{min}$ to fully reduce the oxidized Pd (Figure S3) and to avoid Pd sintering. The operating temperature of CO chemisorption was maintained at -78°C . The stoichiometric ratio of adsorbed CO to exposed Pd atom was assumed to be 1:1, as reported in other researches [41,42]. The mean particle sizes of Pd were calculated according to the relation between the dispersion and the particle size. The Pd 3d and B 1s X-ray photoelectron spectroscopy (XPS) spectra were acquired by using K-alpha (Thermo Scientific Inc, U.K) with Al $\text{K}\alpha$ μ -focused monochromatic (1486.6 eV), operated at 12 kV voltage and 3 mA current. All catalysts were analyzed without any further treatment except the exposure under ambient atmosphere at 100°C for 16 h during the synthetic process. Energy calibration was applied to all spectra by adjusting the binding energy of C 1s at 284.5 eV. The Pd K-edge X-ray absorption fine structure (XAFS) data of the catalyst were collected from 7D-XAFS beamline of Pohang Light Source (PLS-II) at the Pohang Accelerator Laboratory (South Korea), where Si (111) crystal was used as a monochromator with 2.5 GeV beam energy and 300 mA ring current. The energy calibration was performed by Pd-foil with $E_0 = 24,350$ eV. The Pd K-edge X-ray signal was collected at the room temperature by using ionization chambers purged with pure N_2 gas to measure the energies of incident (I_0) and fluorescence (I_f) beams. The step and duration time for X-ray absorption near edge structure (XANES) and extended X-ray absorption fine structure (EXAFS) were 1.0 eV and 2 s, and 0.30 nm^{-1} and 3 s, respectively. The total number of points per the spectrum (i.e. 478) was sufficient for the EXAFS analysis, and the obtained data were analyzed using the Athena (Demeter, U.S.A.). The

cryogenic hydrogen temperature programmed reduction (H₂-TPR) was performed by the BEL-CAT-II (BEL Japan Inc.). About 0.03 g of sample was dehydrated in a flow of N₂ at 100 °C for 1 h, and then the temperature was raised from –90 °C to the target temperature with the ramping rate of 10 °C/min while the samples were exposed to 5 vol.% H₂/Ar. Temperature-programmed hydride decomposition (TPHD) analysis was also performed in the BEL-CAT-II (BEL Japan Inc.) after reducing the sample by pretreatment under 5 vol.% H₂/Ar gas condition at 100 °C for 0.5 h with the ramping rate of 10 °C/min. Then, TCD-signal was recorded under a flowing condition of 5 vol.% H₂/Ar gas while raising the temperature from 0 °C to 150 °C with the ramping rate of 10 °C/min.

2.3. Catalytic reaction

The reaction system was equipped with a two-necked glass reactor, one of whose necks was sealed with a rubber septum while the other was connected to a burette filled with oil. Typically, 0.05 g of the catalyst was loaded in the reactor before the reaction. The reactor was heated, and its temperature was maintained at each reaction temperature in a water bath. In order to equilibrate the temperature of reactant at the reaction temperature, 10 mL of 1 M formic acid was placed in an oven for 1 h before the reaction. The reaction started as soon as the formic acid solution was introduced into the reactor through the rubber septum by a syringe. As most of the products from the FAD reaction were the gaseous phase, the generated gas extruded the oil in the burette. The amount of extruded oil was measured by a compacted balance concurrently recording the mass value at every 3 s. As the mass value could be converted into the volumetric value by the density of oil, the volumetric amount of generated gas was measured. The reliability and reproducibility of the reaction system were confirmed by the repeated reaction tests over commercial Pd/C catalyst (Figure S4).

The generated gas from the FAD reaction was analyzed by FT-IR spectrometer (Nicolet iS50, Thermo Scientific) with a 3 m gas cell in order to check if only the dehydrogenation of formic acid occurred during the reaction. The FT-IR spectra confirmed the absence of CO gas in the product (Figure S5), demonstrating that there was no dehydration reaction of formic acid under our condition.

2.4. TOF calculation

The turnover frequency (TOF) values were calculated on the basis of the total number of Pd atoms (bulk Pd) and the number of active Pd atoms (surface of Pd). The TOF (h^{−1}, bulk) based on the total number of Pd atoms was calculated as follows: $TOF(h^{-1}, bulk) = \frac{(P \cdot V) / (R \cdot T)}{2N \cdot t}$ (mol_{gas} mol_{Pd}^{−1} h^{−1}), where P is the atmospheric pressure (1 atm), V is the generated gas volume of 0.01 L, R is the gas constant (0.082 L·atm·K^{−1} mol^{−1}), T is the room temperature (298 K), N is the total number of Pd in 0.05 g of the catalyst, and t is the reaction time required to obtain the generated gas of 0.01 L immediately after the stabilization. In order to rule out other factors determining the activity (e.g. decrease of reactant concentration or Pd sintering), such initial activity (V/t) was adopted. The TOF (h^{−1}, surface) per active Pd atoms was calculated in the following: $TOF(h^{-1}, surface) = \frac{(P \cdot V) / (R \cdot T)}{2N \cdot D \cdot t}$ (h^{−1}), where all parameters are the same as above, while D is the dispersion of Pd of the catalyst. The dispersions of Pd in the catalysts were obtained indirectly from the particle size from TEM images by applying the following equation: [43–45] $D(\%) = \frac{(6 \times C_a \times m \times 10^3)}{(\rho \times d \times N_A)} \times 100$, where C_a is the concentration of surface metal atoms (Pd: 1.27 × 10¹⁹ atoms/m²), m is the atomic weight of metal (Pd: 106.42 g/mol), ρ is the metal density (Pd: 1.202 × 10⁷ g/m³), d is the average particle size obtained from TEM (nm), and N_A is Avogadro's number (6.02 × 10²³ atoms/mol). The dispersions of Pd were also acquired directly from CO chemisorption.

Table 1

Pd contents, average particle sizes, dispersions, and surface areas of the size-controlled Pd/C catalysts depending on the number of NaBH₄ treatments.

	Pd (wt. %) ¹	Size (nm) ²	Standard deviation (nm) ²	Size (nm) ³	Dispersion (%) ³	S _{BET} (m ² /g) ⁴
Pd/C-0T	6.5	2.5	0.48	2.4	45.8	190
Pd/C-1T	6.6	3.3	0.64	3.3	34.0	193
Pd/C-2T	6.6	3.7	0.81	3.8	29.5	195
Pd/C-3T	6.6	4.2	1.00	4.4	25.4	199
Pd/C-4T	6.6	4.8	1.11	5.0	22.4	201

¹ obtained from ICP-AES, ² calculated from TEM images, ³ analyzed by CO chemisorption, ⁴ obtained from N₂ adsorption-desorption isotherm by BET calculation.

3. Results and discussion

3.1. Physicochemical properties of the size-controlled Pd/C catalysts

The size-controlled Pd/C catalysts prepared by changing the number of NaBH₄ treatments were investigated by using various characterization methods. As shown in Table 1, all catalysts contained a similar Pd loading of 6.5 ± 0.1 wt.% (ICP-AES), approximately equal to the expected content of 6.6 wt.%. Fig. 1 displays typical TEM images of the size-controlled Pd/C catalysts and their particle size distributions with average particle sizes. The average particle sizes of Pd increased with increasing the number of NaBH₄ treatments from 0 to 4. Such result was attributed to the sintering of the Pd particles due to the *in-situ* generated hydrogen from NaBH₄ and the sufficient temperature (60 °C) where oxidized Pd is reduced (Figure S3). The distributions of the particle sizes in Fig. 1 become broad with the number of NaBH₄ treatments, but there is no bimodal distribution in any samples. This indicates that the particles were generally sintered to form large particles, not partially aggregated. The CO chemisorption was also performed to obtain the dispersions of Pd in the catalysts, where the average particle sizes were also calculated. As presented in Table 1, when the catalysts underwent the NaBH₄ treatment, the dispersions of Pd decreased, while the average particle sizes increased. The XRD patterns show the characteristic peaks of metallic Pd at around 40.1°, 46.5°, 67.9° and 82.1° (Figure S6). The main peak at 40.1° was used in the Scherrer equation to obtain the crystallite sizes of Pd, which are also displayed in Figure S6. Although the crystallite sizes are not accurate due to the overlapping with other peaks arising from carbon support, a trend of the crystallite sizes matched well with the results of TEM and CO chemisorption. Fig. 2 represents the Fourier transformed EXAFS of the size-controlled samples with those of reference PdO and Pd metal. The relative small peak intensities of the samples, compared to the reference PdO and Pd metal, was attributed to their small Pd size. While Pd-O and Pd-Pd peaks were observed at around 1.6 Å and 2.6 Å, respectively, there was no Pd-O-Pd peak at around 3.1 Å originating from bulk PdO. This indicates that the Pd particles were not oxidized in a bulk phase. The intensity of Pd-Pd peak increased with the number of NaBH₄ treatments, whereas the intensity of Pd-O peak slightly decreased. It also demonstrates that the size of Pd increased with the number of NaBH₄ treatments. To sum up, we could conclude that the size-controlled Pd/C catalysts were well synthesized with the various average Pd sizes.

Fig. 3 displays the XPS spectra in the Pd 3d region of the size-controlled Pd/C catalysts. The Pd 3d_{5/2} and 3d_{3/2} of spectra could be deconvoluted into mainly two peaks, Pd(0) and Pd(II). The peak corresponding to Pd(0) appeared at around 335.6 eV, while the peak of Pd (II) did at around 336.8 eV. The relative peak intensity of Pd(0) continuously increased from Pd/C-0T to Pd/C-4T, whereas that of Pd(II) diminished. The relative peak areas and the peak positions of Pd(0) and Pd(II) were quantitatively measured, and listed in Table 2. The

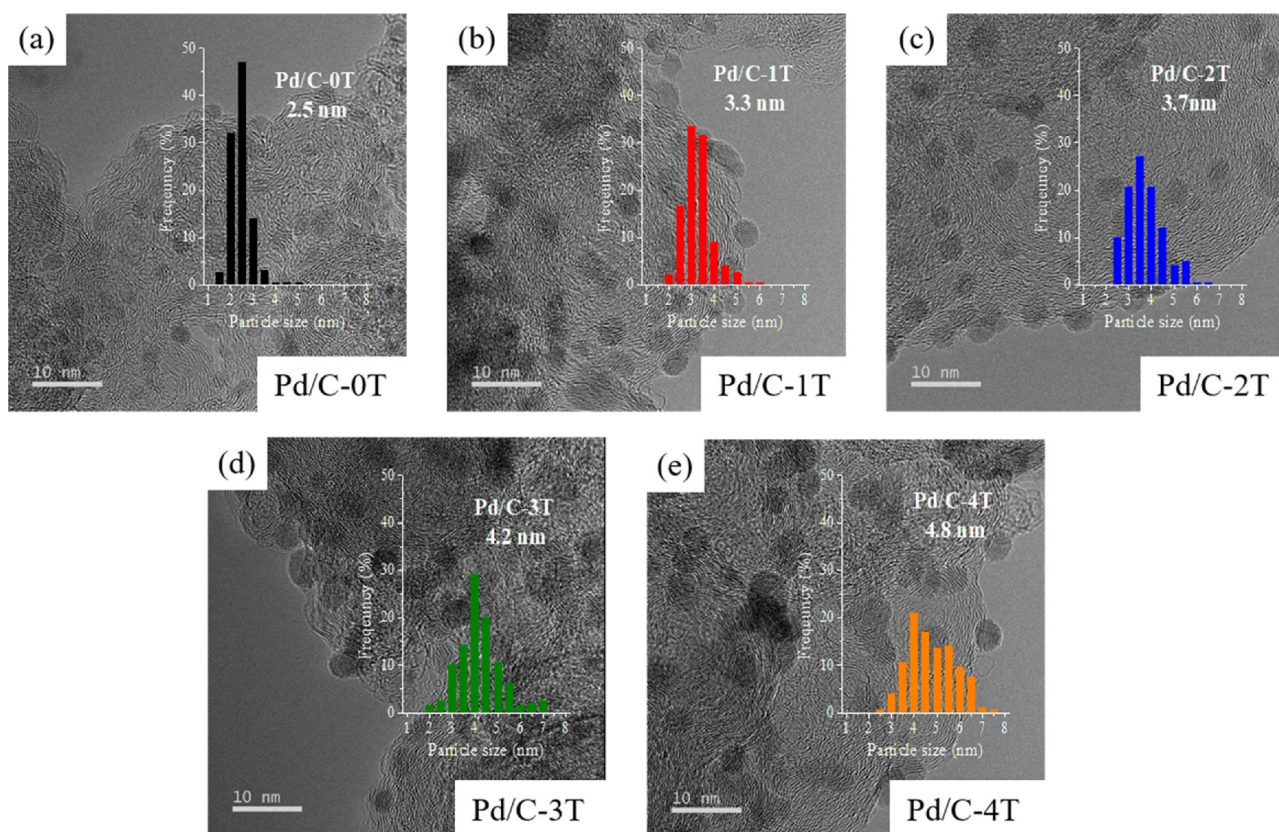


Fig. 1. Representative TEM images and particle size distributions with average particle sizes of (a) Pd/C-0T, (b) Pd/C-1T, (c) Pd/C-2T, (d) Pd/C-3T, and (e) Pd/C-4T.

proportion of Pd (II) decreased with the increase in the Pd size, consistent with the results of other researches. [39,40,46,47] The dependence of the oxidation state on the Pd size was also evidenced by Pd XANES (Figure S7). Specifically, while the Pd XANES spectrum of Pd/C-0T was close to that of the reference PdO, those of Pd/C-xT catalysts with the increase in the x value approached to that of Pd metal. Meanwhile, in Fig. 2, the absence of Pd-O-Pd peak (at around 3.1 Å) and the presence of Pd-O peak underline that only a few surface layers of Pd were oxidized near the surface without forming bulk PdO. Thus, we could conclude that the Pd(II) species in the catalyst originated from the unstable Pd species near the surface of the particle, since the unstable Pd (e.g. near-surface atoms with low-coordination number) tends to lower its high energy through the reaction with oxygen under oxidizing condition. However, the peak positions of all catalysts in XPS spectra were maintained at around 335.5 eV and 336.9 eV for Pd(0) and Pd(II), respectively (Table 2). Those unchanged binding energy values indicate that there is no noticeable d-band shift among the size-

controlled Pd/C catalysts with the Pd size from 2.5 nm to 4.8 nm.

It should be noted that the oxidation state of Pd identified by XPS and XANES could not represent the Pd phase during the reaction, as the oxidized Pd species in the catalyst would be reduced to the metallic Pd during the reaction. This is not only because the FAD reaction is the hydrogen evolving reaction, but also because the oxidized Pd species in all catalysts are completely reduced under hydrogen atmosphere even at the temperature of 30 °C (Figure S8), which was the lowest reaction temperature we chose. In order to investigate whether the presence of oxidized Pd species in the prepared catalyst affects the overall catalytic activity or not, the FAD reaction was tested over the size-controlled Pd/C catalysts before and after the reduction at 30 °C (Figure S9), and their initial activities are displayed in Fig. 4. Since the catalysts were exposed under 5 vol.% of H₂/Ar for 1 h at the temperature of 30 °C during the reduction, all oxidized Pd species in the catalysts were reduced to the metallic Pd based on the H₂-TPR results (Figure S8). However, there was no significant difference in the catalytic activity before and after

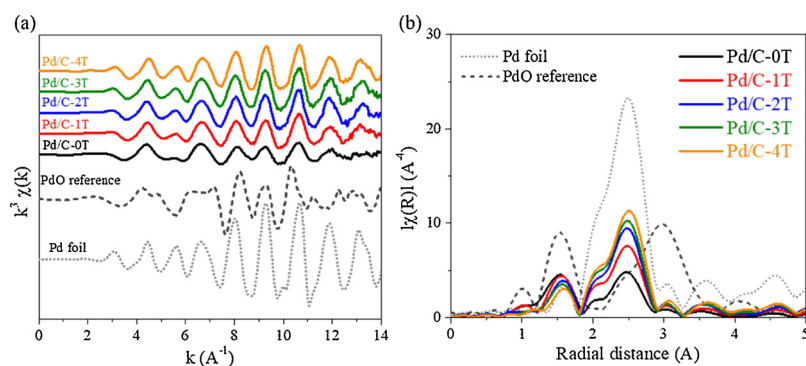


Fig. 2. (a) EXAFS oscillations of k^3 -weighted Pd K-edge and (b) their Fourier transforms for Pd foil, PdO bulk reference, and the size-controlled Pd/C catalysts.

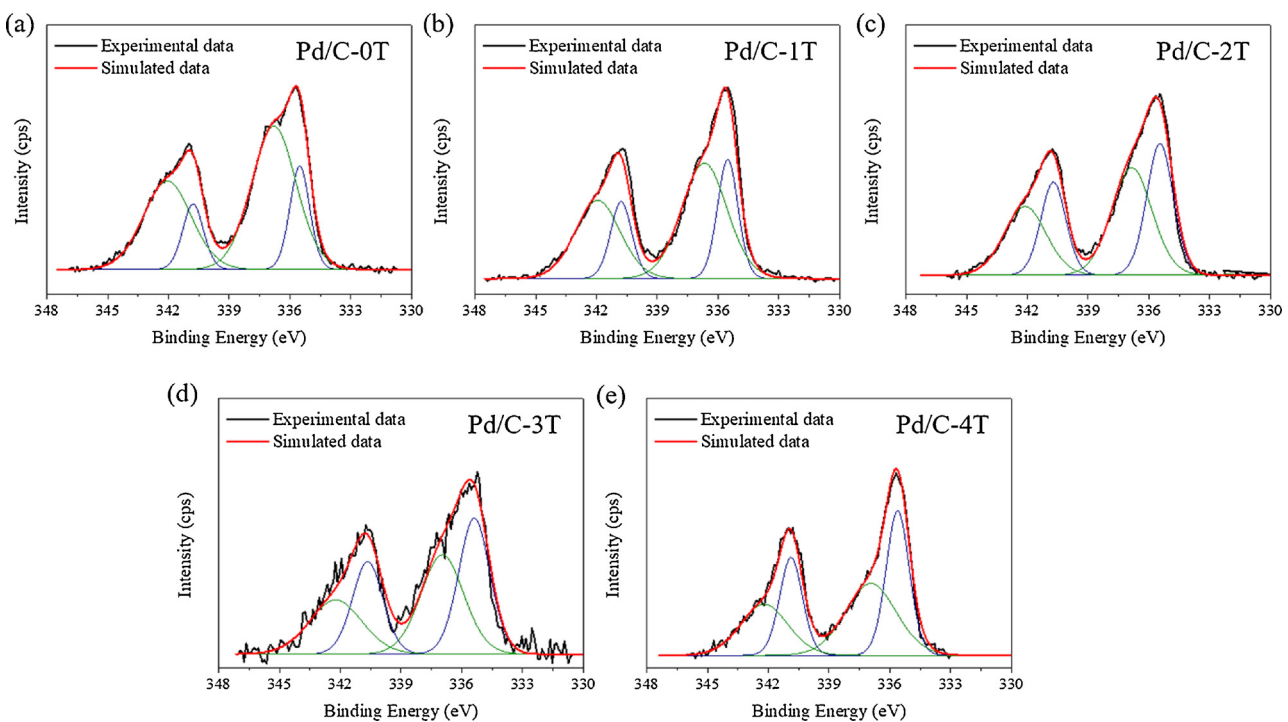


Fig. 3. XPS spectra in Pd 3d region and their deconvoluted spectra of (a) Pd/C-0T, (b) Pd/C-1T, (c) Pd/C-2T, (d) Pd/C-3T, and (e) Pd/C-4T.

Table 2

Relative peak areas and binding energies of Pd° and Pd^{2+} according to the deconvoluted XPS spectra of the size-controlled Pd/C catalysts.

	Pd/C-0T	Pd/C-1T	Pd/C-2T	Pd/C-3T	Pd/C-4T
Pd° (%)	24.3	31.8	44.6	49.8	60.0
Pd^{2+} (%)	75.7	68.2	55.4	50.2	40.0
Pd° (eV)	335.5	335.5	335.5	335.4	335.5
Pd^{2+} (eV)	336.8	336.7	336.8	336.8	336.8

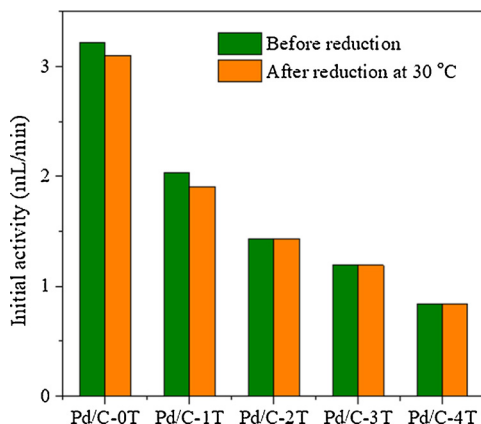


Fig. 4. Initial activities for the formic acid dehydrogenation reaction (10 mL 1 M formic acid at the temperature of 30 °C) over the size-controlled Pd/C catalysts before and after the reduction at 30 °C for 1 h.

the reduction. This result indicates that the oxidized Pd is reduced as soon as the reaction occurs, and thus the presence of oxidized Pd species in the prepared catalysts barely affects the catalytic activity of FAD. Corresponding to our result, Lu et al. observed that the catalytic activity was nearly maintained after the reduction at 25 °C, although there was a deactivation after the reduction at 200 °C [39]. Chan et al. also reported that there was no obvious difference in the activity of Pd/C catalyst before and after the reduction [13]. Hence, the effect of the

oxidized Pd species present in the prepared catalysts would be neglected when explaining the Pd size effect on the FAD reaction.

The surface areas of the size-controlled Pd/C catalysts were calculated from the N_2 adsorption-desorption isotherm (Figure S10), and are summarized in Table 1. The surface area of the carbon support declined from $213 \text{ m}^2/\text{g}$ to $190 \text{ m}^2/\text{g}$ when the 6.5 wt.% of the smallest Pd particles were loaded on carbon in the case of Pd/C-0 T. However, as the catalysts underwent the several numbers of NaBH_4 treatment, the surface area continuously increased from $190 \text{ m}^2/\text{g}$ of Pd/C-0 T to $201 \text{ m}^2/\text{g}$ of Pd/C-4 T. It is because, after the Pd sintering, N_2 was accessible to the small pores that the small Pd particles had occupied. Nevertheless, the effect of surface areas on the catalytic activity is expected to be negligible, as evidenced by their small difference between the size-controlled Pd/C catalysts ($< 11 \text{ m}^2/\text{g}$). The presence of boron (B) on the catalyst surface was also investigated by applying XPS analysis. Cai et al. and Studt et al. through experimental and theoretical approaches, respectively, reported that boron can boost the catalytic activity of Pd/C catalyst for hydrogen production from formic acid [48,49]. Although boron was possibly present in the size-controlled Pd/C catalysts due to the NaBH_4 treatments, the XPS results confirmed that none of boron existed on the catalyst surface after the filtration with excess water (Figure S11). Hence, the promoting effect of boron can also be excluded.

3.2. Effect of particle size on catalytic activity

The catalytic activities of the size-controlled Pd/C catalysts were evaluated by performing the reaction with 1 M 10 mL formic acid at each reaction temperature. The temperature was varied from 30 °C to 60 °C in order to thermodynamically understand the Pd size effect on FAD. Fig. 5 shows the volumes of generated gas during the reaction as a function of reaction time at the reaction temperature of 30 °C, 40 °C, 50 °C and 60 °C. The Pd/C-0 T catalyst having the smallest Pd size exhibited the highest catalytic activity in the entire temperature range, and the catalytic activity declined as the Pd size increased. Because the total number of exposed sites on the surface increases with the decrease in the particle size, the largest number of active sites in Pd/C-0 T could

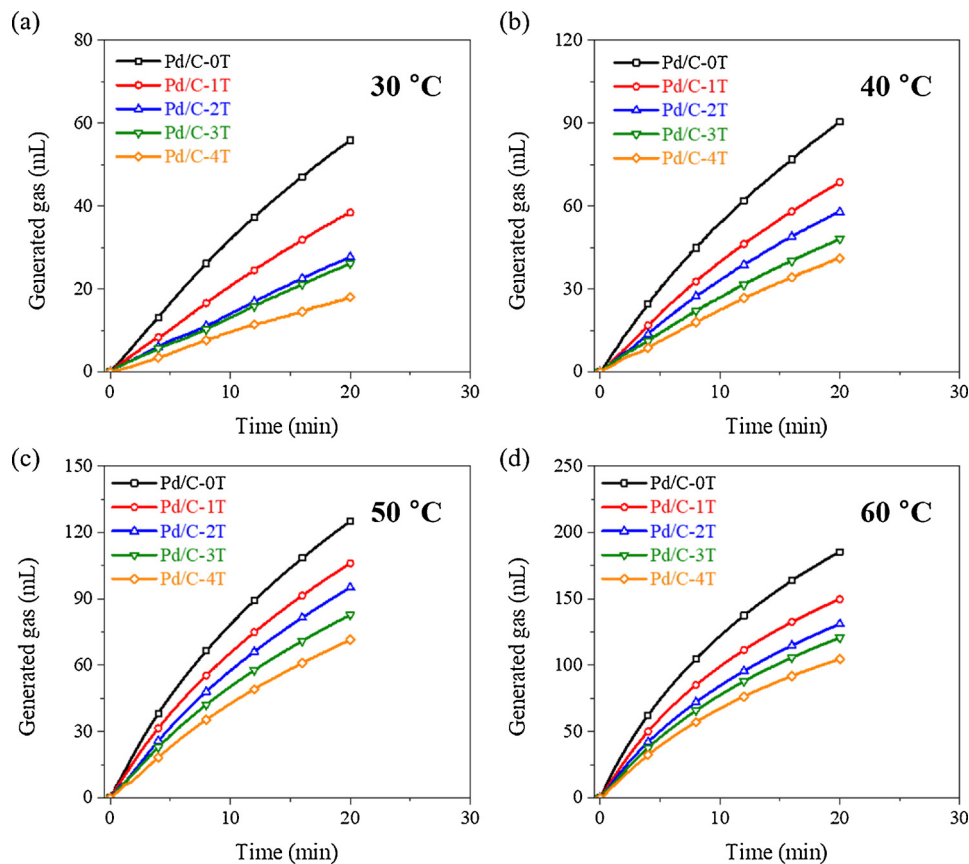


Fig. 5. Volumes of generated gases during the reaction with 10 mL 1 M formic acid at the temperatures of (a) 30 °C, (b) 40 °C, (c) 50 °C and (d) 60 °C without any additive over 0.05 g of the size-controlled Pd/C catalysts (3 mM of Pd).

easily explain the highest catalytic activity among the size-controlled samples. However, since the performance of the catalyst is determined not only by the number of active sites but also by the intrinsic activity of active sites, it is also essential to calculate the turnover frequency (TOF).

The TOF values were calculated in terms of the total number of Pd and the number of surface Pd sites in the catalysts, which were named as TOF (h^{-1} , bulk) and TOF (h^{-1} , surface), respectively (Figures S12 and S13). Then, the TOF values were normalized based on the TOF values of Pd/C-0 T to compensate for the difference in TOF values between the catalysts originating from the reaction temperature. The correlation between the normalized values and the Pd size are shown in Fig. 6. The normalized TOF (h^{-1} , bulk) values exhibited the decreasing trend with increasing the Pd size at all reaction temperatures, in line with the catalytic activities (Fig. 5). However, the normalized TOF (h^{-1} , surface) values showed different trends depending on the reaction temperature. At the low temperature of 30 °C and 40 °C, the normalized TOF (h^{-1} , surface) values continuously decreased with the increase of the Pd size similar to the normalized TOF (h^{-1} , bulk). This is consistent with other previous researches [39,40]. Interestingly, such decreasing trends of the normalized TOF values with increasing Pd size at the low temperature seem to highlight that the small Pd catalyst facilitates the reaction more actively than the large Pd catalyst. Cai et al. explained that the size-dependent activity for FAD with Pd size from 2.0 nm to 5.2 nm was attributed to either the accumulation of poisonous species (e.g. CO) or the changes in C–H bond dissociation step due to σ -band shift, but without providing concrete evidence [40]. Moreover, since any shift of Pd binding energy representing σ -band shift was not identified by the XPS analysis (Table 2), the σ -band shift effect can be ruled out in our Pd size range from 2.5 nm to 4.8 nm. Meanwhile, it is more important to note that the normalized TOF (h^{-1} , surface) values

demonstrated comparably independent trends regarding the Pd size at the high temperature above 50 °C. Such temperature-dependent result clearly implies that there is a significant thermodynamic effect of Pd size on FAD. Furthermore, the same conclusion was obtained when calculating TOF values from CO chemisorption (Figures S13 and S14) or when applying the cuboctahedron model (Figures S15 and S16).

The chemical reaction is closely related to the reaction temperature, because it needs sufficient energy to be activated. Thus, it is a significant fact that the decreasing trend of the normalized TOF values depending on Pd size gradually vanished when the reaction temperature rose. In order to clarify the thermodynamic effects of Pd size on FAD, the catalytic activities were correlated with the reaction temperature by using the Arrhenius equation. Fig. 7 represents the Arrhenius plots of size-controlled Pd/C catalysts. The apparent activation energies, calculated from the Arrhenius equation, gradually increased from 44.9 kJ/mol of Pd/C-0 T to 63.9 kJ/mol of Pd/C-4 T, as the Pd size of the catalysts increased. The activation energies of the catalysts indicate that the catalyst with the large Pd size requires higher energy to activate the FAD reaction. Moreover, such activation energies elucidate the disappearance of decreasing TOF trend depending on the Pd size when raising the reaction temperature in Fig. 6, because the difference between the reaction rates with high and low activation energies diminishes as the reaction temperature increases.

As it was identified that the small Pd catalyst has high activity due to both the number of active sites and thermodynamic factor, we tried to differentiate the thermodynamic effect and the number of active sites effect at each reaction temperature. Fig. 8 shows the TOF (h^{-1} , bulk) values of Pd/C-0 T, Pd/C-4 T and corrected Pd/C-4 T depending on the reaction temperature. For the purpose of matching the number of active sites in Pd/C-0 T and Pd/C-4 T catalysts, the catalytic activity of Pd/C-4 T catalyst was multiplied by the dispersion ratio of Pd/C-0 T

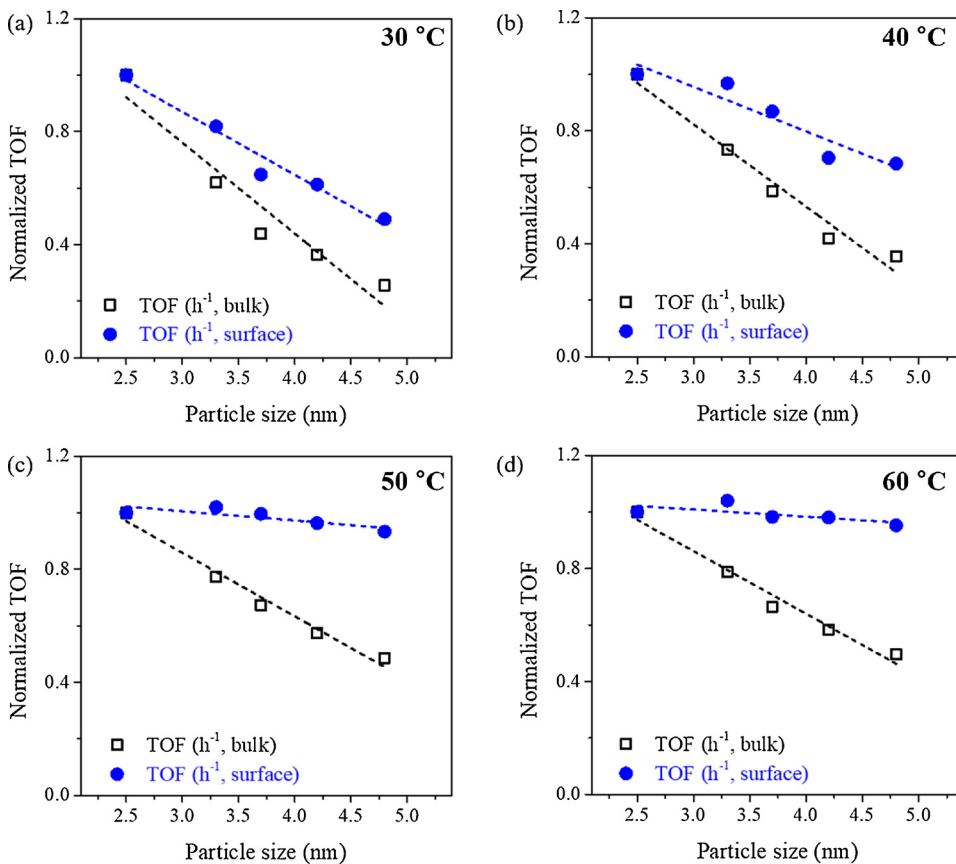


Fig. 6. Two kinds of the normalized turnover frequency (TOF) values per total number of active metal atoms (bulk) and the number of active sites (surface) as a function of the particle size obtained from TEM images at the temperature of (a) 30 °C, (b) 40 °C, (c) 50 °C and (d) 60 °C. The values were normalized based on the TOF values of Pd/C-0T.

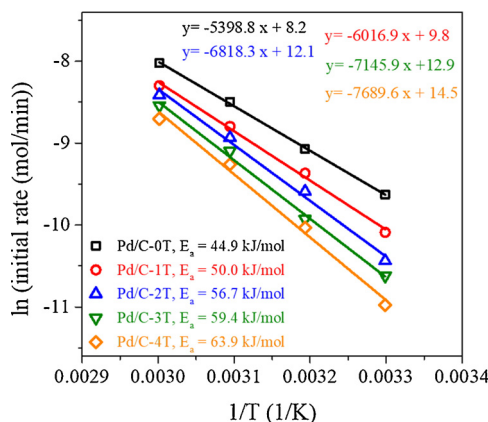


Fig. 7. The Arrhenius plots between temperatures and initial activities of the size-controlled Pd/C catalysts in the temperature range from 30 °C to 60 °C, and their activation energies obtained from the Arrhenius equation.

catalyst to Pd/C-4 T catalyst (Figure S17), which was nominated as the corrected Pd/C-4 T ($= \text{Pd/C-4 T values} \times (\text{D}_{\text{Pd/C-0T}}/\text{D}_{\text{Pd/C-4T}})$). Since the numbers of active sites in the Pd/C-0 T catalyst and the corrected Pd/C-4 T were the same, the difference between TOF (h^{-1} , bulk) values of Pd/C-0 T and the corrected Pd/C-4 T solely represents the thermodynamic effect of the Pd size (blue-slash bar). On the other hand, the difference between TOF (h^{-1} , bulk) values of Pd/C-4 T and corrected Pd/C-4 T simply indicates the effect of the number of active sites (orange-slash bar). Hence, by comparing TOF values, both the thermodynamic effect of the Pd size and the effect of the number of active sites could be distinguished. As the reaction temperature rose, the difference between Pd/C-0 T and corrected Pd/C-4 T continuously decreased, indicating that the thermodynamic effect of the Pd size on the catalytic activity is reduced with increasing the temperature, as

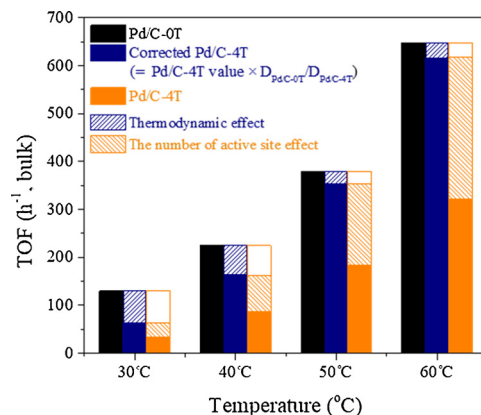
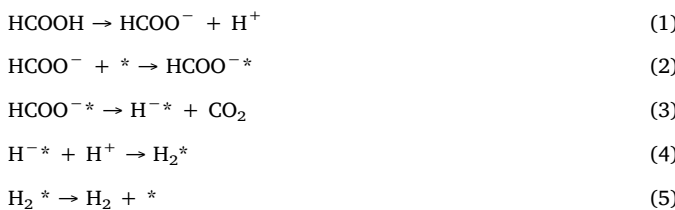


Fig. 8. Turnover frequency (TOF) values per total number of active metal atoms (bulk) of Pd/C-0 T, Pd/C-4T and corrected Pd/C-4 T whose number of active sites is corrected by that of Pd/C-0T ($= \text{Pd/C-4 T values} \times \text{D}_{\text{Pd/C-0T}}/\text{D}_{\text{Pd/C-4T}}$).

mentioned in the previous paragraph. Contrary to the thermodynamic effect, the number of active sites affects the catalytic activity more significantly at the higher reaction temperature as marked in the orange-slash bar in Fig. 8. It was attributed to the significant improvement of intrinsic activity of the active site when raising the reaction temperature. Consequently, we could conclude that the catalytic activity of Pd/C catalyst at the low temperature was largely affected by the thermodynamic effect, while the number of active sites influences the catalytic activity more dominantly at the high temperature.

The activation energy was largely dependent on the Pd size in Fig. 7. As the activation energy is determined by the rate-determining step, the size-dependent activity needs understanding in respect to the reaction pathway. The pathway for the FAD reaction in the aqueous phase was proposed as follows [9,50–52]



In detail, formic acid is first deprotonated in the aqueous phase. Next, the thus formed formate ion is absorbed on Pd, and then decomposed into hydride (H^-) and CO_2 . Because it is well known that Pd can store hydrogen in the form of hydride [53], the hydride can be adsorbed stably on Pd. The hydride is combined with proton/hydronium ion in water to generate hydrogen. Finally, hydrogen molecule desorbs from the active site.

A kinetic isotope effect (KIE) study was generally used to identify the rate-determining step of reaction. Through the KIE study for FAD, several groups concluded that C–H bond dissociation step is the rate-determining step, because they observed the decrease in initial activity when substituting the reactant from formic acid (HCOOH) to formic-d acid (DCOOH) [38,54–56]. However, many of them also observed the decrease of initial activity when using formic acid-d (HCOOD) instead of HCOOH with the reaction order of $\text{HCOOH} + \text{H}_2\text{O} > \text{HCOOD} + \text{H}_2\text{O} > \text{DCOOH} + \text{H}_2\text{O}$ [38,54,55]. In another investigation by Asefa et al., the replacement of the solvent from H_2O to deuterium oxide (D_2O) significantly deteriorated the initial activity, indicating that not only HCOO^- but also H_2O is involved in the rate-determining step [57]. However, the decline of the reaction rate when replacing H_2O to D_2O or HCOOH to HCOOD cannot be explained by adopting the C–H dissociation step as the rate-determining step. It is more reasonable to propose that step (4) or (5) is the rate-determining step of FAD, as all deuteriums originating from HCOOD, DCOOH and even D_2O can degenerate the reaction rates of steps (4) and (5). Moreover, since the step (4) is energetically spontaneous reaction [58,59], the hydrogen desorption step (step (5)) is suggested as the rate-determining step for FAD reaction. It can explain the different reaction rate depending on the origins of deuterium (e.g. HCOOD, DCOOH and D_2O). Deuterium dissociated from HCOOD forms hydronium ion with one deuterium (H_2DO^+), whereas deuterium from D_2O solvent forms hydronium ion with two deuterium (HD_2O^+). Thus, the number of deuterium participates in the step (5) is larger in D_2O case than in HCOOD case. In contrast, while not all deuterium is involved in the step (5) due to competitive usage with hydrogen in step (4) when using HCOOD or D_2O , all deuterium from DCOOH adsorbs on the active site as shown in steps (2) and (3). As a result, the proportion of deuterium participating in step (5) is the highest when deuterium originates from DCOOH, followed by D_2O and HCOOD. Thus, the proposal about the hydrogen desorption step ($\text{H}_2^* \rightarrow \text{H}_2 + *$) as the rate-determining step expiates the KIE results much better than the suggestion of C–H cleavage as the rate-determining step.

Recently, Yamashita et al. also reported that the H_2 desorption step is the rate-determining step for FAD based on theoretical and experimental studies [60]. In another study, they claimed that one effect of N-functional group to improve the catalytic activity is to promote the H_2 desorption step [61]. Since we proposed that the H_2 desorption step is the rate-determining step of the FAD reaction, the promotion of catalytic activity with decreasing the Pd size might originate from the Pd size-dependent H_2 desorption behavior. In order to identify the size dependence of H_2 desorption behavior, temperature-programmed hydride decomposition (TPHD) analysis was carried out over the size-controlled Pd/C catalysts, whose results are presented in Fig. 9. The negative peak in TPHD profiles originates from the thermal decomposition of Pd-hydride complex (PdH_x) [24,62]. The temperature of PdH_x decomposition continuously rose from 50 °C to 55 °C with Pd size, indicating the large Pd needs the higher energy than small Pd to

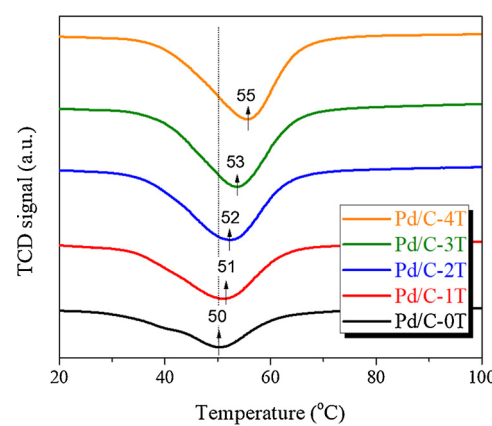


Fig. 9. Temperature-programmed hydride decomposition (TPHD) profiles of the size-controlled Pd/C catalysts.

decompose PdH_x . Such size-dependent decomposition temperature of PdH_x was also observed by Nag, evidenced by the continuous increases of the decomposition temperature of PdH_x with the crystallite size of Pd on carbon in the range from about 2.5 to 11 nm [53]. Specifically, the PdH_x decomposition temperature rose by about 5 °C when Pd size increased from 2.5 nm to 5 nm, consistent with our result [53]. Recently, Zhou et al. also adopted TPHD analysis as a probe reaction of combinative desorption of hydrogen, and obtained similar TPHD profiles over the size-controlled Pd/TiO₂ catalysts [59]. They theoretically and experimentally proved that the H_2 desorption is the rate-determining step of combinative desorption of hydrogen, and moreover, H_2 desorption is lagged by the Pd size enlargement [59]. Thus, their explanation that large Pd requires higher energy to desorb H_2 elucidates the phenomena that the large size Pd has the high PdH_x decomposition temperature in Fig. 9 [59].

The activation energy and H_2 desorption temperature are depicted as a function of the Pd size in Fig. 10. It clearly shows the similar dependences of the activation energy and the PdH_x decomposition temperature on the Pd size, both of which increased with the Pd size. The H_2 desorption step was suggested as the rate-determining step of FAD by understanding KIE results. In addition, the H_2 desorption step requires the higher energy when Pd becomes larger, which was demonstrated by the TPHD analysis. Hence, as the large size Pd requires the high energy to desorb H_2 from Pd, it also needs the high energy to dehydrogenate formic acid. This explains why the activity and activation energy of the size-controlled Pd/C catalysts were dependent on the Pd size. To sum up, it can be concluded that the size-dependent catalytic activity of FAD is attributed not only to the number of active sites but also to the rate-determining step governing the activation energy. The understanding of the Pd size effect on the FAD about the rate-

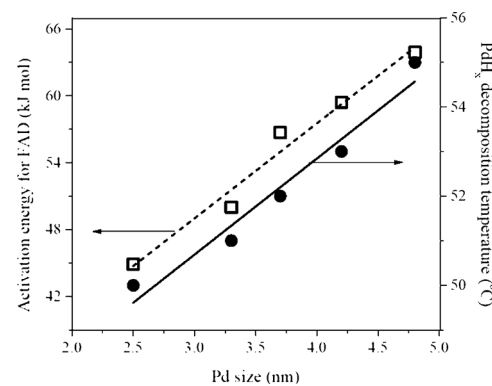


Fig. 10. The activation energies of formic acid dehydrogenation and the decomposition temperatures of PdH_x depending on the Pd size.

determining step would provide a clue to improve catalytic activity by lowering the H₂ desorption energy from Pd.

4. Conclusion

The size-controlled Pd/C catalysts were prepared by applying a deposition-precipitation method and by controlling the number of NaBH₄ treatments. The TEM analysis informed that the particle sizes of Pd were controlled well from 2.5 nm to 4.8 nm, which was also supported by other characterization methods such as CO chemisorption, XRD patterns and EXAFS. The catalytic activity for FAD was improved when the catalyst has a small Pd size, which is typically attributed to a large number of active sites. However, TOF (h⁻¹, surface) values decreased with the Pd size at low temperature, while such decreasing trend disappeared at high temperature. It indicates the thermodynamic effect of Pd size on the FAD reaction, in addition to the effect of the number of active sites. Such results can be explained by size-dependent activation energies of FAD, which varied from 44.9 kJ/mol to 63.9 kJ/mol with the Pd size. Moreover, the H₂ desorption step is suggested as the rate-determining step. This elucidates the changes in the activation energy depending on the Pd size, which is supported by TPHD analysis. As a result, through the investigation on the effect of the Pd size on FAD, lowering the hydrogen desorption energy of Pd is proposed as a way to improve the catalytic activity.

Acknowledgements

This research was supported by Basic Science Research Program through the National Research Foundation of Korea (NRF) funded by the Ministry of Science, ICT & Future Planning (MSIP) (NRF-2016R1A5A1009592). The experiments at PLS-II were also supported in part by the Ministry of Science, ICT, and Future Planning (MSIP) and the Pohang University of Science and Technology (POSTECH).

Appendix A. Supplementary data

Supplementary material related to this article can be found, in the online version, at doi:<https://doi.org/10.1016/j.apcatb.2018.12.008>.

References

- [1] T.C. Johnson, D.J. Morris, M. Wills, Hydrogen generation from formic acid and alcohols using homogeneous catalysts, *Chem. Soc. Rev.* 39 (2010) 81–88.
- [2] K.V. Kordesch, G.R. Simader, Environmental impact of fuel cell technology, *Chem. Rev.* 95 (1995) 191–207.
- [3] M. Grasemann, G. Laurenczy, Formic acid as a hydrogen source - recent developments and future trends, *Energy Environ. Sci.* 5 (2012) 8171–8181.
- [4] L.J. Jia, D.A. Bulushev, S. Beloshapkin, J.R.H. Ross, Hydrogen production from formic acid vapour over a Pd/C catalyst promoted by potassium salts: evidence for participation of buffer-like solution in the pores of the catalyst, *Appl. Catal. B* 160 (2014) 35–43.
- [5] D.A. Bulushev, S. Beloshapkin, J.R.H. Ross, Hydrogen from formic acid decomposition over Pd and Au catalysts, *Catal. Today* 154 (2010) 7–12.
- [6] M. Zacharska, A.L. Chuvilin, V.V. Kriventsov, S. Beloshapkin, M. Estrada, A. Simakov, D.A. Bulushev, Support effect for nanosized Au catalysts in hydrogen production from formic acid decomposition, *Catal. Sci. Technol.* 6 (2016) 6853–6860.
- [7] F. Solymosi, Á. Koós, N. Liliom, I. Ugrai, Production of CO-free H₂ from formic acid. A comparative study of the catalytic behavior of Pt metals on a carbon support, *J. Catal.* 279 (2011) 213–219.
- [8] Z. Li, X. Yang, N. Tsumori, Z. Liu, Y. Himeda, T. Autrey, Q. Xu, Tandem nitrogen functionalization of porous carbon: toward immobilizing highly active palladium nanoclusters for dehydrogenation of formic acid, *ACS Catal.* 7 (2017) 2720–2724.
- [9] K. Mori, M. Dojo, H. Yamashita, Pd and Pd–Ag nanoparticles within a macroreticular basic resin: an efficient catalyst for hydrogen production from formic acid decomposition, *ACS Catal.* 3 (2013) 1114–1119.
- [10] H.J. Jeon, Y.M. Chung, Hydrogen production from formic acid dehydrogenation over Pd/C catalysts: Effect of metal and support properties on the catalytic performance, *Appl. Catal. B* 210 (2017) 212–222.
- [11] J.-K. Sun, W.-W. Zhan, T. Akita, Q. Xu, Toward homogenization of heterogeneous metal nanoparticle catalysts with enhanced catalytic performance: soluble porous organic cage as a stabilizer and homogenizer, *J. Am. Chem. Soc.* 137 (2015) 7063–7066.
- [12] S. Jones, A. Kolpin, S.C.E. Tsang, Modification of Pd for formic acid decomposition by support grafted functional groups, *Catal. Struct. React.* 1 (2015) 19–24.
- [13] C.Q. Hu, J.K. Puller, S.W. Ting, K.Y. Chan, Activity of Pd/C for hydrogen generation in aqueous formic acid solution, *Int. J. Hydrogen Energy* 39 (2014) 381–390.
- [14] Z.L. Wang, J.M. Yan, H.L. Wang, Y. Ping, Q. Jiang, Pd/C synthesized with citric acid: an efficient catalyst for hydrogen generation from formic acid/sodium formate, *Sci. Rep.* 2 (2012) 598.
- [15] D. Ruthven, The catalytic decomposition of aqueous formic acid over suspended palladium catalysts, *J. Catal.* 21 (1971) 39–47.
- [16] K. Tedree, C.W. Chan, S. Jones, Q. Cuan, W.K. Li, X.Q. Gong, S.C. Tsang, (1)(3)C NMR guides rational design of nanocatalysts via chemisorption evaluation in liquid phase, *Science* 332 (2011) 224–228.
- [17] Z. Li, Q. Xu, Metal-nanoparticle-catalyzed hydrogen generation from formic acid, *Acc. Chem. Res.* 50 (2017) 1449–1458.
- [18] Y. Huang, X. Zhou, M. Yin, C. Liu, W. Xing, Novel PdAu@Au/C core – shell catalyst: superior activity and selectivity in formic acid decomposition for hydrogen generation, *Chem. Mater.* 22 (2010) 5122–5128.
- [19] C.Y. Hu, X.L. Mu, J.M. Fan, H.B. Ma, X.J. Zhao, G.X. Chen, Z.Y. Zhou, N.F. Zheng, Interfacial effects in PdAg bimetallic nanosheets for selective dehydrogenation of formic acid, *ChemNanoMat* 2 (2016) 28–32.
- [20] C. Feng, Y.H. Hao, L. Zhang, N.Z. Shang, S.T. Gao, Z. Wang, C. Wang, AgPd nanoparticles supported on zeolitic imidazolate framework derived N-doped porous carbon as an efficient catalyst for formic acid dehydrogenation, *RSC Adv.* 5 (2015) 39878–39883.
- [21] M. Yurderi, A. Bulut, M. Zahmakiran, M. Kaya, Carbon supported trimetallic PdNiAg nanoparticles as highly active, selective and reusable catalyst in the formic acid decomposition, *Appl. Catal. B* 160 (2014) 514–524.
- [22] X. Zhou, Y. Huang, W. Xing, C. Liu, J. Liao, T. Lu, High-quality hydrogen from the catalyzed decomposition of formic acid by Pd-Au/C and Pd-Ag/C, *Chem. Commun. (Camb.)* (2008) 3540–3542.
- [23] Y.L. Qin, Y.C. Liu, F. Liang, L.M. Wang, Preparation of Pd-Co-based nanocatalysts and their superior applications in formic acid decomposition and methanol oxidation, *ChemSusChem* 8 (2015) 260–263.
- [24] Y. Kim, J. Kim, D.H. Kim, Investigation on the enhanced catalytic activity of a Ni-promoted Pd/C catalyst for formic acid dehydrogenation: effects of preparation methods and Ni/Pd ratios, *RSC Adv.* 8 (2018) 2441–2448.
- [25] Y. Karatas, A. Bulut, M. Yurderi, I.E. Ertas, O. Alal, M. Gulcan, M. Celebi, H. Kivrak, M. Kaya, M. Zahmakiran, PdAu-MnOx nanoparticles supported on amine-functionalized SiO₂ for the room temperature dehydrogenation of formic acid in the absence of additives, *Appl. Catal. B* 180 (2016) 586–595.
- [26] N. Caner, A. Bulut, M. Yurderi, I.E. Ertas, H. Kivrak, M. Kaya, M. Zahmakiran, Atomic layer deposition-SiO₂ layers protected PdCoNi nanoparticles supported on TiO₂ nanopowders: exceptionally stable nanocatalyst for the dehydrogenation of formic acid, *Appl. Catal. B* 210 (2017) 470–483.
- [27] L. Yang, X. Hua, J. Su, W. Luo, S. Chen, G. Cheng, Highly efficient hydrogen generation from formic acid-sodium formate over monodisperse AgPd nanoparticles at room temperature, *Appl. Catal. B* 168–169 (2015) 423–428.
- [28] A. Bulut, M. Yurderi, Y. Karatas, M. Zahmakiran, H. Kivrak, M. Gulcan, M. Kaya, Pd-MnOx nanoparticles dispersed on amine-grafted silica: highly efficient nanocatalyst for hydrogen production from additive-free dehydrogenation of formic acid under mild conditions, *Appl. Catal. B* 164 (2015) 324–333.
- [29] J.-M. Yan, Z.-L. Wang, L. Gu, S.-J. Li, H.-L. Wang, W.-T. Zheng, Q. Jiang, AuPd-MnOx/MOF-graphene: an efficient catalyst for hydrogen production from formic acid at room temperature, *Adv. Energy Mater.* 5 (2015) 1500107-n/a.
- [30] M. Navlani-Garcia, M. Martis, D. Lozano-Castello, D. Cazorla-Amoros, K. Mori, H. Yamashita, Investigation of Pd nanoparticles supported on zeolites for hydrogen production from formic acid dehydrogenation, *Catal. Sci. Technol.* 5 (2015) 364–371.
- [31] M. Hattori, H. Einaga, T. Daio, M. Tsuji, Efficient hydrogen production from formic acid using TiO₂-supported AgPd@Pd nanocatalysts, *J. Mater. Chem. A* 3 (2015) 4453–4461.
- [32] A. Bulut, M. Yurderi, Y. Karatas, Z. Say, H. Kivrak, M. Kaya, M. Gulcan, E. Ozensoy, M. Zahmakiran, MnOx-promoted PdAg alloy nanoparticles for the additive-free dehydrogenation of formic acid at room temperature, *ACS Catal.* 5 (2015) 6099–6110.
- [33] J. Cheng, X. Gu, P. Liu, H. Zhang, L. Ma, H. Su, Achieving efficient room-temperature catalytic H₂ evolution from formic acid through atomically controlling the chemical environment of bimetallic nanoparticles immobilized by isoreticular amine-functionalized metal-organic frameworks, *Appl. Catal. B* 218 (2017) 460–469.
- [34] S. Akbayrak, Y. Tonbul, S. Ozkar, Nanoceria supported palladium(0) nanoparticles: Superb catalyst in dehydrogenation of formic acid at room temperature, *Appl. Catal. B* 206 (2017) 384–392.
- [35] H. Dai, B. Xia, L. Wen, C. Du, J. Su, W. Luo, G. Cheng, Synergistic catalysis of AgPd@ZIF-8 on dehydrogenation of formic acid, *Appl. Catal. B* 165 (2015) 57–62.
- [36] H. Dai, N. Cao, L. Yang, J. Su, W. Luo, G. Cheng, AgPd nanoparticles supported on MIL-101 as high performance catalysts for catalytic dehydrogenation of formic acid, *J. Mater. Chem. A* 2 (2014) 11060–11064.
- [37] Q.-L. Zhu, N. Tsumori, Q. Xu, Immobilizing extremely catalytically active palladium nanoparticles to carbon nanospheres: a weakly-capping growth approach, *J. Am. Chem. Soc.* 137 (2015) 11743–11748.
- [38] M. Navlani-Garcia, K. Mori, A. Nozaki, Y. Kuwahara, H. Yamashita, Investigation of size sensitivity in the hydrogen production from formic acid over carbon-supported pd nanoparticles, *Chemistryselect* 1 (2016) 1879–1886.
- [39] J. Li, W. Chen, H. Zhao, X. Zheng, L. Wu, H. Pan, J. Zhu, Y. Chen, J. Lu, Size-dependent catalytic activity over carbon-supported palladium nanoparticles in

dehydrogenation of formic acid, *J. Catal.* 352 (2017) 371–381.

[40] S. Zhang, B. Jiang, K. Jiang, W.B. Cai, Surfactant-free synthesis of carbon-supported palladium nanoparticles and size-dependent hydrogen production from formic acid-formate solution, *ACS Appl. Mater. Interfaces* 9 (2017) 24678–24687.

[41] Y. Zhao, L. Jia, J.A. Medrano, J.R.H. Ross, L. Lefferts, Supported Pd catalysts prepared via colloidal method: the effect of acids, *ACS Catal.* 3 (2013) 2341–2352.

[42] S.B. Kang, I.S. Nam, B.K. Cho, C.H. Kim, S.H. Oh, Universal activity function for predicting performance of Pd-based TWC as function of Pd loading and catalyst mileage, *Chem. Eng. J.* 259 (2015) 519–533.

[43] S.B. Kang, H.J. Kwon, I.S. Nam, Y.I. Song, S.H. Oh, Activity function for describing alteration of three-way catalyst performance over palladium-only three-way catalysts by catalyst mileage, *Ind. Eng. Chem. Res.* 50 (2011) 5499–5509.

[44] D. Roth, P. Gelin, A. Kaddouri, E. Garbowksi, M. Primet, E. Tena, Oxidation behaviour and catalytic properties of Pd/Al2O3 catalysts in the total oxidation of methane, *Catal. Today* 112 (2006) 134–138.

[45] C.A. Müller, M. Maciejewski, R.A. Koeppe, A. Baiker, Combustion of methane over palladium/zirconia: effect of Pd-particle size and role of lattice oxygen, *Catal. Today* 47 (1999) 245–252.

[46] W.J. Zhou, J.Y. Lee, Particle size effects in Pd-catalyzed electrooxidation of formic acid, *J. Phys. Chem. C* 112 (2008) 3789–3793.

[47] W.J. Zhou, M. Li, O.L. Ding, S.H. Chan, L. Zhang, Y.H. Xue, Pd particle size effects on oxygen electrochemical reduction, *Int. J. Hydrogen Energy* 39 (2014) 6433–6442.

[48] K. Jiang, K. Xu, S. Zou, W.-B. Cai, B-Doped Pd catalyst: boosting room-temperature hydrogen production from formic acid-formate solutions, *J. Am. Chem. Soc.* 136 (2014) 4861–4864.

[49] J.S. Yoo, Z.J. Zhao, J.K. Norskov, F. Studt, Effect of boron modifications of palladium catalysts for the production of hydrogen from formic acid, *ACS Catal.* 5 (2015) 6579–6586.

[50] F.Z. Song, Q.L. Zhu, N. Tsumori, Q. Xu, Diamine-alkalized reduced graphene oxide: immobilization of Sub-2 nm palladium nanoparticles and optimization of catalytic activity for dehydrogenation of formic acid, *ACS Catal.* 5 (2015) 5141–5144.

[51] X. Wang, G.-W. Qi, C.-H. Tan, Y.-P. Li, J. Guo, X.-J. Pang, S.-Y. Zhang, Pd/C nanocatalyst with high turnover frequency for hydrogen generation from the formic acid–formate mixtures, *Int. J. Hydrogen Energy* 39 (2014) 837–843.

[52] M.A. Ziaeef, H. Zhong, C. Cui, R. Wang, Additive-free hydrogen generation from formic acid boosted by amine-functionalized imidazolium-based ionic polymers, *ACS Sustain. Chem. Eng.* (2018).

[53] N.K. Nag, A study on the formation of palladium hydride in a carbon-supported palladium catalyst, *J. Phys. Chem. B* 105 (2001) 5945–5949.

[54] M. Kohsuke, T. Hiromasa, D. Masahiro, Y. Kazunari, Y. Hiromi, Synergic catalysis of PdCu alloy nanoparticles within a macroreticular basic resin for hydrogen production from formic acid, *Chem. Eur. J.* 21 (2015) 12085–12092.

[55] K. Koh, M. Jeon, C.W. Yoon, T. Asefa, Formic acid dehydrogenation over Pd NPs supported on amine-functionalized SBA-15 catalysts: structure-activity relationships, *J. Mater. Chem. A* 5 (2017).

[56] K. Tedesree, T. Li, S. Jones, C.W. Chan, K.M. Yu, P.A. Bagot, E.A. Marquis, G.D. Smith, S.C. Tsang, Hydrogen production from formic acid decomposition at room temperature using a Ag-Pd core-shell nanocatalyst, *Nat. Nanotechnol.* 6 (2011) 302–307.

[57] K. Koh, M. Jeon, D.M. Chevrier, P. Zhang, C.W. Yoon, T. Asefa, Novel nanoporous N-doped carbon-supported ultrasmall Pd nanoparticles: efficient catalysts for hydrogen storage and release, *Appl. Catal. B* 203 (2017) 820–828.

[58] S.J. Blanksby, G.B. Ellison, Bond dissociation energies of organic molecules, *Acc. Chem. Res.* 36 (2003) 255–263.

[59] J. Wang, H.Y. Tan, D. Jiang, K.B. Zhou, Enhancing H-2 evolution by optimizing H adatom combination and desorption over Pd nanocatalyst, *Nano Energy* 33 (2017) 410–417.

[60] S. Masuda, K. Mori, Y. Futamura, H. Yamashita, PdAg nanoparticles supported on functionalized mesoporous carbon: promotional effect of surface amine groups in reversible hydrogen delivery/storage mediated by formic acid/CO₂, *ACS Catal.* 8 (2018) 2277–2285.

[61] M. Navlani-Garcia, D. Salinas-Torres, K. Mori, A.F. Léonard, Y. Kuwahara, N. Job, H. Yamashita, Insights on palladium decorated nitrogen-doped carbon xerogels for the hydrogen production from formic acid, *Catal. Today* (2018).

[62] S.B.C. Pergher, R.M. Dallago, R.C. Veses, C.E. Gigola, I.M. Baibich, Pd/NaY-zeolite and Pd-W/NaY-zeolite catalysts: preparation, characterization and NO decomposition activity, *J. Mol. Catal. A Chem.* 209 (2004) 107–115.